Cross-sectional design of a composite rotor blade for twist morphing

Mohammadreza Amoozgar, Alexander D. Shaw, Jiaying Zhang, Michael I. Friswell

College of Engineering, Swansea University, Swansea SA1 8EN, United Kingdom

Abstract

In this paper, a systematic and reliable approach is presented to design a composite rotor blade cross-section with high in-plane bending-torsion coupling. The composite blade is designed to allow changing of the twist of the blade in flight, actuated by a moving proof mass near the tip of the blade. By shifting the mass along the chord of the blade, a variable bending moment is obtained. This bending moment can change the twist of the blade through the bend-twist coupling. First a baseline composite blade spar is selected, and the effect of various parameters on the different cross-sectional properties and the rotating frequencies of the blade are investigated. Then, the optimized cross-section with high bend-twist coupling is determined. It is found that the skin ply angle, skin thickness, and the spar location have significant effect on the coupling, with the strongest sensitivity being the skin ply angle.

Introduction

Morphing technology is the study of changing the aircraft characteristics to enhance the performance of the vehicle, or to reduce its environmental impact (1). There are several concepts introduced in the literature for morphing the aircraft wing to improve the overall performance of the aircraft (2). The morphing concepts may change the shape locally on the section of the wing, or globally on the wing platform. Reed et al. (3) developed a morphing mechanism to change the chord length of the section. They used sliding ribs to alter the chordwise location of the trailing and leading edges. A smart leading-edge section has been designed by Kintscher et al. (4), and showed that this mechanism is able to produce high lift performance. Woods and Friswell (5) introduced a novel morphing section inspired by nature known as the Fishbone Active Camber. They showed that this concept has the potential to enhance the aerodynamic performance of the wing. A variable span wing has been developed by Vale et al. (6) to reduce the aerodynamic drag.

Rotorcraft have many operational advantages over fixed wing aircraft (7). To improve the rotorcraft design to be more environmentally friendly in terms of low levels of pollution, noise, and fuel consumption, and high levels of comfort and performance, morphing rotor blades have been proposed. Chen and Chopra (8, 9) studied and tested the twist change of a blade by using the piezoelectric actuators. They showed that by locating the piezoelectric patches on the upper and lower surfaces, about 0.4^o twist change at the 4 rev^{-1} condition was achieved. They showed also that about 10% increase in the rotor lift is achievable by 0.6^o linear twist change. The advantages and disadvantages of several morphing concepts introduced for vibration reduction have been summarized by Straub and Chopra (10, 11). Chattopadhyay et al. (12) used the active damping layer to improve the aeromechanical stability of rotors. The results highlighted the importance of the number of actuators and their location on the dynamic load reduction. Dynamic behaviour of rotor blades with an active twist mechanism for reduction of noise and vibration has been analysed by Cesnik et al. (13). The blade was equipped with anisotropic strain actuators embedded in the composite layers, and the bench and hover tests were carried out. The analytical results showed a very good correlation with experimental results. This study was further developed to check the developed analytical model for the forward flight condition (14). Thakkar and Ganguli (15) developed an analytical model for a rotor blade with piezoelectric material. They concluded that shear actuation has more effect on the rotor response than a bending actuator. Schultz (16) presented a new concept based on bi-stable structures for large shape morphing and at the same time with low energy input. In this concept, two curved shells were attached together to make a section with two stable configurations. Twist modification of a tiltrotor blade by using a shape memory alloy torque tube was proposed by Prahlad and Chopra (17). It was shown that the heat treatment of the shape memory alloys affects the actuation behaviour. Bushnell et al. (18) developed and tested an active twist rotor blade based on shape memory alloys. Pagano et al. (19) considered two morphing strategies aiming to mitigate the environmental impact of the helicopter flight. These first strategy was to optimize the aerodynamic of the blade through the camber change of the section by an actuator, while the second one strategy was to modify the twist of the blade by using an SMA rod. Changing the twist of the helicopter blade by a using a warp-induced concept was proposed by Mistry et al. (20). In this concept, by warping the skin with the help of rotating a threaded rod attached to the skin near the trailing edge of

the blade, the twist changes. Mistry and Gandhi (21) presented the design to test of a variable camber blade based on a warp-induced concept. They showed that 18^o camber variation over a 45 in span blade with a warping actuation of 0.18 in length is feasible. Amoozgar et al. (22) proposed a new concept for changing the twist of a composite blade in flight. In this concept, by moving a mass located near the tip of the blade, a torsional moment through the bend-twist coupling presented in the composite layup was obtained. Therefore, the twist of the blade was related to the point mass movement.

Rotor blade design is a complex and multidisciplinary task which combines aerodynamics, dynamics, structures, and acoustics together (23). The blade design can be divided into local and global levels of optimization (24). In the latter level, the aerodynamic, aeroelastic, and acoustic behaviour of the blade is obtained, while in the former level of optimization, the layout and the material distribution of the cross-section is determined. Li et al. (24) presented a new method for cross-sectional design of composite rotor blades. A parametric cross-section was introduced and the effect of different design parameters on the various cross-sectional properties was obtained, however the composite couplings weren't considered. Cesnik et al. (25) presented a framework for designing an active twist rotor blade with embedded anisotropic piezocomposite actuators. This framework was applied to optimize a cross-section that maximizes the twist actuation of the blade. Glaz et al. (26) introduced a surrogate-based optimization approach to design a helicopter blade with low levels of vibration. In this study, first a baseline composite blade was obtained, and then it was optimized to reduce the vibration of the rotor blade.

In this study, which is a continuation of the authors previous study (22), a composite cross-section capable of producing high amount of bend-twist coupling is presented. A baseline blade resembling the BO-105 main rotor blade is introduced, and then the design is modified to have high bend-twist coupling. To achieve this aim, the composite blade structure is modelled by using a 1D geometrically exact fully intrinsic beam equations combined with a detailed 2D cross-sectional analysis tool. Then a parametric cross-section composed of several components is considered, and the effect of each component on the bend-twist coupling is evaluated. Then by using the generic algorithm, the optimized design sections have been determined.

Problem Statements

In this study a composite hingeless rotor blade rotating with a constant velocity is considered, and the goal is to design a cross-section relevant to the proposed morphing proposal.

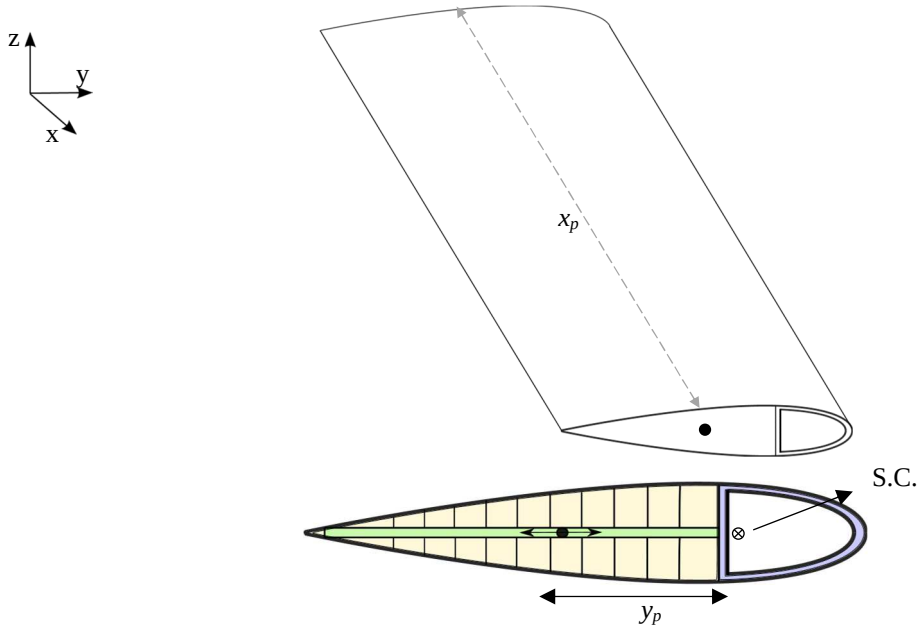

Figure 1: Schematic of the twist morphing concept

In this morphing concept, the change in the blade twist is the result of moving a mass and the composite tailoring. Figure 1 shows a tailored composite blade with a movable mass. The length of the blade is R, the point mass is denoted by m_p, and its location is determined by x_p, y_p, z_p. x_p is measured from the root of the blade, and y_p is the

offset of the point mass from the shear centre of the cross-section. It is noted that in this study it is considered that the point mass offset in the thickness direction is zero ($z_p=0$).
Adding a mass to the blade will produce an extra centrifugal force. This centrifugal force can turn to a bending moment when the mass moves in the chordwise direction of the section. This in-plane bending moment could then change the twist of the blade through the bend-twist coupling of the tailored composite blade. As the bend-twist coupling of the composite spar has the main contribution in the morphing concept, therefore the main goal of this study is to first assess what are the effective parameters, and then to design a cross-section with high bend-twist coupling.

Formulation

The composite hingeless rotor blade is modelled here by combining a 1D elastic beam with a 2D cross-sectional analysis tool. The beam behaviour is simulated by the geometrically exact fully intrinsic beam equations (27), which has been used successfully for modelling beam-like structures (28-32):

$$\partial F_1/\partial x_1 + K_2F_3 - K_3F_2 = \partial P_1/\partial t + \Omega_2P_3 - \Omega_3P_2$$

$$\partial F_2/\partial x_1 + K_3F_1 - K_1F_3 = \partial P_2/\partial t + \Omega_3P_1 - \Omega_1P_3$$

$$\partial F_3/\partial x_1 + K_1F_2 - K_3F_1 = \partial P_3/\partial t + \Omega_1P_2 - \Omega_2P_1$$

$$\partial M_1/\partial x_1 + K_2M_3 - K_3M_2 + 2\gamma_{12}F_3 - 2\gamma_{13}F_2 = \partial H_1/\partial t + \Omega_2H_3 - \Omega_3H_2 + V_2P_3 - V_3P_2$$

$$\partial M_2/\partial x_1 + K_3M_1 - K_1M_3 + 2\gamma_{13}F_1 - (1+\gamma_{11})F_3 = \partial H_2/\partial t + \Omega_3H_1 - \Omega_1H_3 + V_3P_1 - V_1P_3$$

$$\partial M_3/\partial x_1 + K_1M_2 - K_2M_1 + (1+\gamma_{11})F_2 - 2\gamma_{12}F_1 = \partial H_3/\partial t + \Omega_1H_2 - \Omega_2H_1 + V_1P_2 - V_2P_1$$

$$\partial V_1/\partial x_1 + K_2V_3 - K_3V_2 + 2\gamma_{12}\Omega_3 - 2\gamma_{13}\Omega_2 = \partial\gamma_{11}/\partial t \quad (1)$$

$$\partial V_2/\partial x_1 + K_3V_1 - K_1V_3 - (1+\gamma_{11})\Omega_3 + 2\gamma_{13}\Omega_1 = 2\partial\gamma_{12}/\partial t$$

$$\partial V_3/\partial x_1 + K_1V_2 - K_2V_1 + (1+\gamma_{11})\Omega_2 - 2\gamma_{12}\Omega_1 = 2\partial\gamma_{13}/\partial t$$

$$\partial\Omega_1/\partial x_1 + K_2\Omega_3 - K_3\Omega_2 = \partial\kappa_1/\partial t$$

$$\partial\Omega_2/\partial x_1 + K_3\Omega_1 - K_1\Omega_3 = \partial\kappa_2/\partial t$$

$$\partial\Omega_3/\partial x_1 + K_1\Omega_2 - K_2\Omega_1 = \partial\kappa_3/\partial t$$

where F_i and M_i for i=1,..,3, are the internal forces and moments, V_i and Ω_i are the linear and angular velocities, P_i and H_i are the sectional linear and angular momenta. The generalized strains of the blade are denoted by γ_{1i} and κ_i, and K_i is the final curvature of the deformed beam which is related to the beam curvature through the following relation

$$K_i = \kappa_i + k_i \quad (2)$$

where, k_i for i=1,..,3 is the initial curvature and twist of the beam.
The 2D cross-sectional properties of the blade are determined by using the cross-sectional analysis software, VABS, which has been extensively validated and used in composite beam applications (33). By using VABS, the cross-sectional stiffness of the blade can be obtained. The stiffness matrix then relates the internal forces and moments to the generalized strains through the following relation:

$$\begin{bmatrix} F_1 \\ F_2 \\ F_3 \\ M_1 \\ M_2 \\ M_3 \end{bmatrix} = \begin{bmatrix} A_{11} & A_{12} & A_{13} & B_{11} & B_{12} & B_{13} \\ A_{12} & A_{22} & A_{23} & B_{21} & B_{22} & B_{23} \\ A_{13} & A_{23} & A_{33} & B_{31} & B_{32} & B_{33} \\ B_{11} & B_{12} & B_{13} & D_{11} & D_{12} & D_{13} \\ B_{21} & B_{22} & B_{23} & D_{12} & D_{22} & D_{23} \\ B_{31} & B_{32} & B_{33} & D_{13} & D_{23} & D_{33} \end{bmatrix} \begin{bmatrix} \gamma_{11} \\ 2\gamma_{12} \\ 2\gamma_{13} \\ \kappa_1 \\ \kappa_2 \\ \kappa_3 \end{bmatrix} \quad or \quad \begin{bmatrix} \boldsymbol{F} \\ \boldsymbol{M} \end{bmatrix} = \begin{bmatrix} \boldsymbol{A} & \boldsymbol{B} \\ \boldsymbol{B} & \boldsymbol{D} \end{bmatrix} \begin{bmatrix} \boldsymbol{\gamma} \\ \boldsymbol{\kappa} \end{bmatrix} \quad (3)$$

where **A**, **B**, and **D** are the stiffness components of the composite blade cross-section.

To close the composite blade equations, it is necessary to define the boundary conditions of the blade. The blade is assumed to be a hingeless rotor blade which is completely fixed at the rotor hub and free at the tip. It is also assumed that the rotor speed is constant.

Results and Discussion

In order to assess the sensitivity of different composite spar parameters on the bend-twist coupling, a baseline rotor blade is reproduced for ease of comparison. In this study, a baseline blade that resembles the main rotor blade of the BO-105 is generated. It is assumed that baseline blade has uniform spanwise properties and it is designed to have fundamental frequencies as closely as possible to BO-105 blade. To design the baseline blade, a generic algorithm optimization is used to select the cross-sectional parameters. To achieve this aim a parametric cross-section, as shown in Figure 2, composed of a skin and a D-spar is considered. In this study, the structural characteristics of the blade are more important than the aerodynamic properties, and therefore a symmetric airfoil (NACA0015) is considered here. The rear part of the cross-section behind the spar web is filled with light foam, and the thickness of the skin and the spar are adjustable. The design variables and the design ranges are summarized in Table 1. There are 15 design variables that could be changed during the optimization process. The skin of the blade has two layers, while the D- spar has 5 layers. It is noted that the D-spar front part and rear part have different ply angles, although the thicknesses are the same.

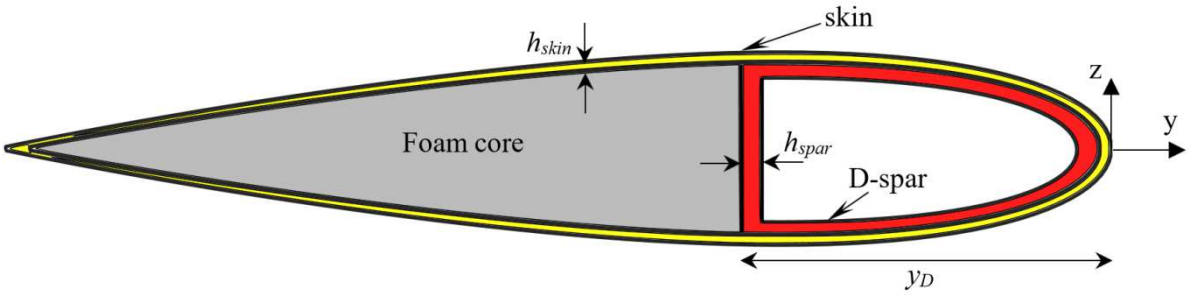

Figure 2: The parametric cross-section of the blade

Table 1: The design variables and the design ranges

Variable name	Design variable	Variable No.	Variable range
skin ply angle (deg)	ζ_1-ζ_2	1-2	[-90,90]
D-spar front part ply angle (deg)	ζ_3-ζ_7	3-7	[-90,90]
D-spar back part ply angle (deg)	ζ_8-ζ_{12}	8-12	[-90,90]
D-spar thickness (mm)	h_D	13	[1,7]
Skin thickness (mm)	h_s	14	[0.5,2]
D-spar location (mm)	y_D	15	[-100,-40]

The cross-section of the blade is meshed adaptively with respect to the design variables. The generated meshes for lower and upper boundaries of the design variable ranges are shown in Figure 3. The BO-105 main rotor blade characteristics are summarized in Table 2.

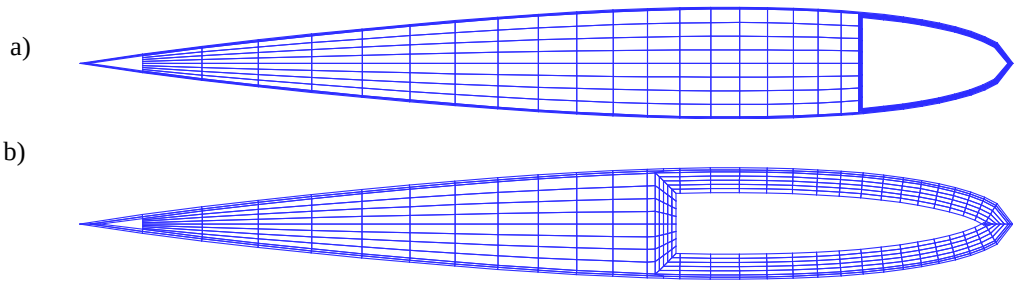

Figure 3: The generated mesh for a) upper boundary and b) lower boundary of design variables

Table 2: Parameters of the BO-105 main rotor blade

Item	Value
Radius (m)	4.9
Chord (m)	0.27
Pre-cone angle (deg)	2.5
Rotating velocity (rad/s)	44.4
1st Lag frequency (/rev)	0.66
1st flap frequency (/rev)	1.12
1st torsion frequency (/rev)	3.6

Baseline design

In this section, the baseline cross-section is designed so that the fundamental frequencies of the baseline blade are as close as possible to the BO-105 main rotor blade. The skin and spar are made of composite material, and the rear part of the spar is filled with Rohacell 51 FX foam. The material properties are presented in Table 3.

Table 3: Material properties of the blade cross-section

property	T300/5208	Foam (Rohacell 51 FX)
E_{11} GPa	181	0.035
$E_{22}= E_{33}$ GPa	10.3	0.035
$G_{12}= G_{13}$ GPa	7.2	0.014
G_{23} GPa	3.9	0.014
ρ kg/m^3	0.28	52
$v_{12}= v_{13}$	0.33	0.25
v_{23}	1600	0.25

At first, the baseline cross-sectional properties are selected by the genetic algorithm so that the fundamental frequencies are as close to the BO-105 blade as possible. The baseline design blade properties are presented in Table 4, and the comparison of the fundamental frequencies between the baseline design and the BO-105 are given in The elastic axis of the baseline design is 2.8% ahead of the quarter chord of the blade, and the mass of the baseline cross-section is 2.4 kg/m. It is noted that as the BO-105 blade mass is 5.55 kg/m and its mass centre is located on the -25% chord, about 2 kg/m mass is added to the blade on -15% of the chord so that the mass centre of the baseline blade coincides with the quarter chord of the blade.

Table 5.

Table 4: Baseline design parameters

Design variable	Value
ζ_1	79^o
ζ_2	63^o
ζ_3	22^o
ζ_4	39^o
ζ_5	73^o
ζ_6	-84^o
ζ_7	37^o
ζ_8	-73^o
ζ_9	85^o
ζ_{10}	-28^o
ζ_{11}	-30^o
ζ_{12}	67^o
h_s	1.5 mm
h_D	4.5 mm
y_D	-49 mm

The elastic axis of the baseline design is 2.8% ahead of the quarter chord of the blade, and the mass of the baseline cross-section is 2.4 kg/m. It is noted that as the BO-105 blade mass is 5.55 kg/m and its mass centre is located on the -25% chord, about 2 kg/m mass is added to the blade on -15% of the chord so that the mass centre of the baseline blade coincides with the quarter chord of the blade.

Table 5: Comparison of the fundamental frequencies of the baseline design and the BO-105 blade

Mode	BO-105	Baseline design
1st lag (/rev)	0.66	0.64
1st flap (/rev)	1.12	1.022
1st torsion (/rev)	3.6	3.69

There are several parameters in the proposed morphing concept, which influence the twist value of the blade. These are the point mass value and location, and bend-twist coupling of the blade (22). As the main objective of this paper is to develop a cross-section with high bend-twist coupling, the rest of the paper is organized so that a cross-section which complies with this morphing concept is determined.

In this study, instead of considering the bend-twist stiffness value directly, a dimensionless parameter named as the nondimensional bend-twist coupling is considered as the objective function of the optimization. This coupling is defined as follows:

$$\alpha = D_{13}/\sqrt{D_{11}.D_{33}}$$

where D_{11}, D_{33}, and D_{13} are the torsional, the bending, and the bend-twist coupling stiffnesses, respectively. This coupling term affects the twist change of the blade dramatically. To this end, the effect of different bend-twist couplings on the tip twist change of the BO-105 blade for various tip masses is shown in Figure 4. In this case, it is assumed that the twist change is the result of moving the point mass from the leading edge to the trailing edge of the blade. It is noted that m_p is the point mass value, μ is the mass per unit length of the blade, and R is the blade span. By increasing the mass ratio, and the nondimensional bend-twist coupling value, the amount of induced twist in the blade increases. Therefore, the nondimensional bend-twist coupling has a direct effect on the amount of twist change in the blade. It is noted that in this morphing concept, the twist distribution along the blade is quadratic with respect to the blade span.

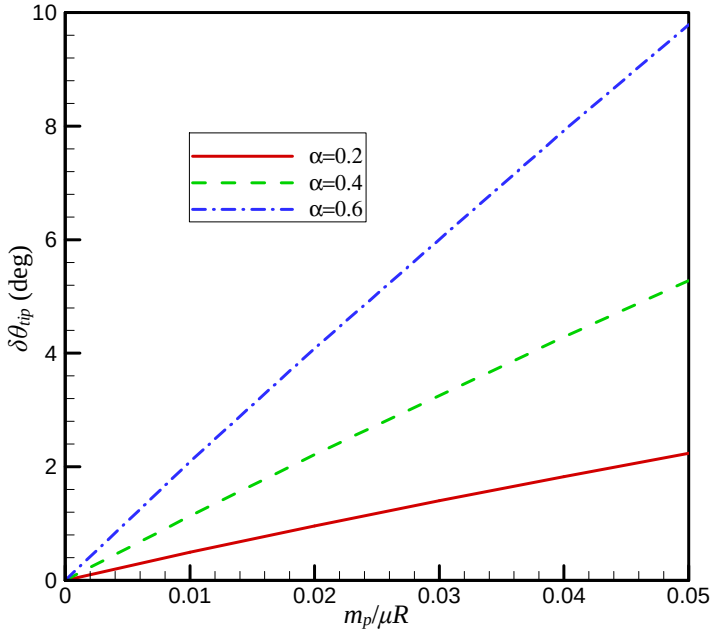

Figure 4: The tip twist change of the BO-105 blade with respect to various values of mass ratios and bend-twist coupling index

In what follows, the sensitivity analysis of different design parameters on the bend-twist coupling is investigated, and finally the best trade-off designs are introduced.

Sensitivity analysis

As the bend-twist coupling of the composite blade influences the proposed morphing concept, in this section, the effect of different cross-sectional parameters on this coupling is investigated. Figure 5 shows the normalized effect of various design parameters mentioned in Table 1 on the bend-twist coupling. The length of each bar in this plot represents the normalized contribution of each design parameter on the coupling in the range of design variables mentioned in Table 1. Almost all the design variables contribute to this coupling, however some of them have a minor effect. The four highest effects belong to the skin ply angles, ζ_1 and ζ_2, skin thickness, and spar location, respectively. It is noted that the skin ply angles contribute more than 80% percent to this coupling.

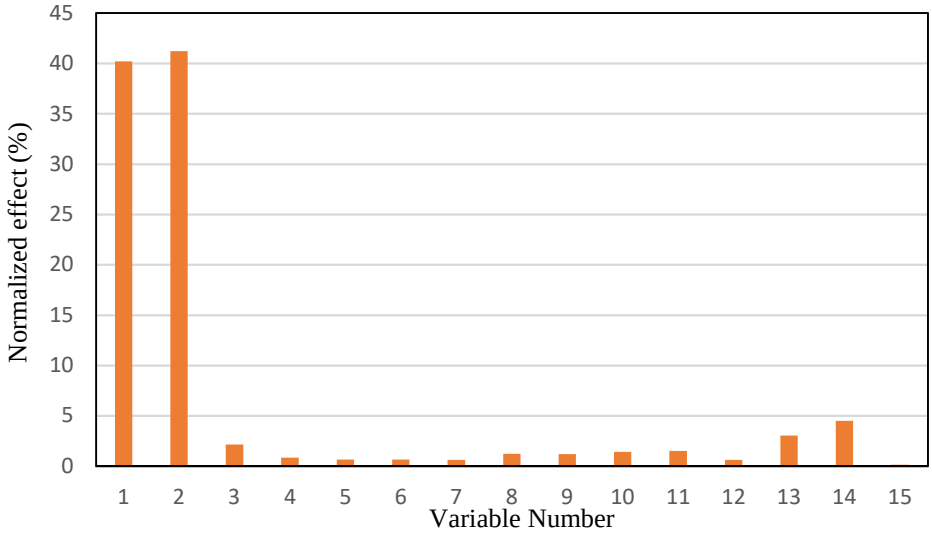

Figure 5: Effect of different design variables on the bend-twist coupling

Figures 6-9 show the mutual effect of two most effective parameters on the bend-twist coupling. Figure 6 shows the effect of the skin first and second layer ply angles on the nondimensional bend-twist coupling. The skin ply angles have significant effects on the coupling, and a certain range of ply angles result to a high bend-twist coupling. In this configuration, the range of the nondimensional coupling value here is between $-0.6 < \alpha < 0.4$.

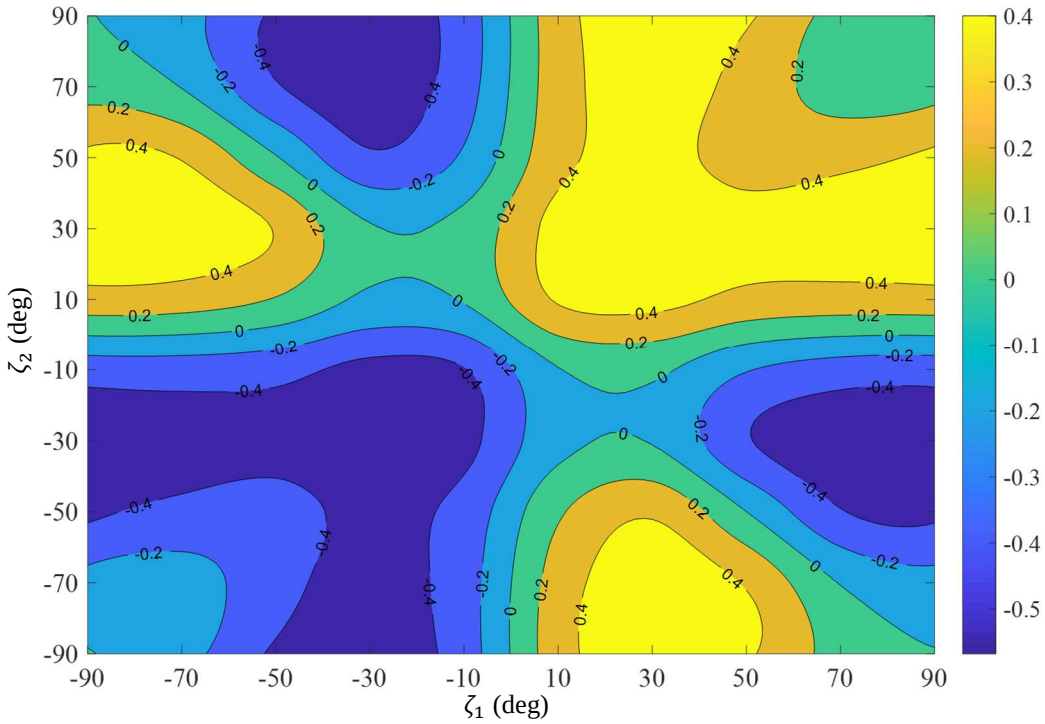

Figure 6: Contour plot of α showing effect of ζ_1 and ζ_2 on the nondimensional bend-twist coupling

The effect of skin ply angle and skin thickness on the nondimensional bend-twist coupling is shown in Figure 7. In this case, the highest coupling takes place in the range of ply angles of $10<\zeta_1<50$ and $-50<\zeta_1<-10$. In contrast, the skin thickness has a direct effect on the coupling value, however the effect is not significant in comparison to the skin ply angle.

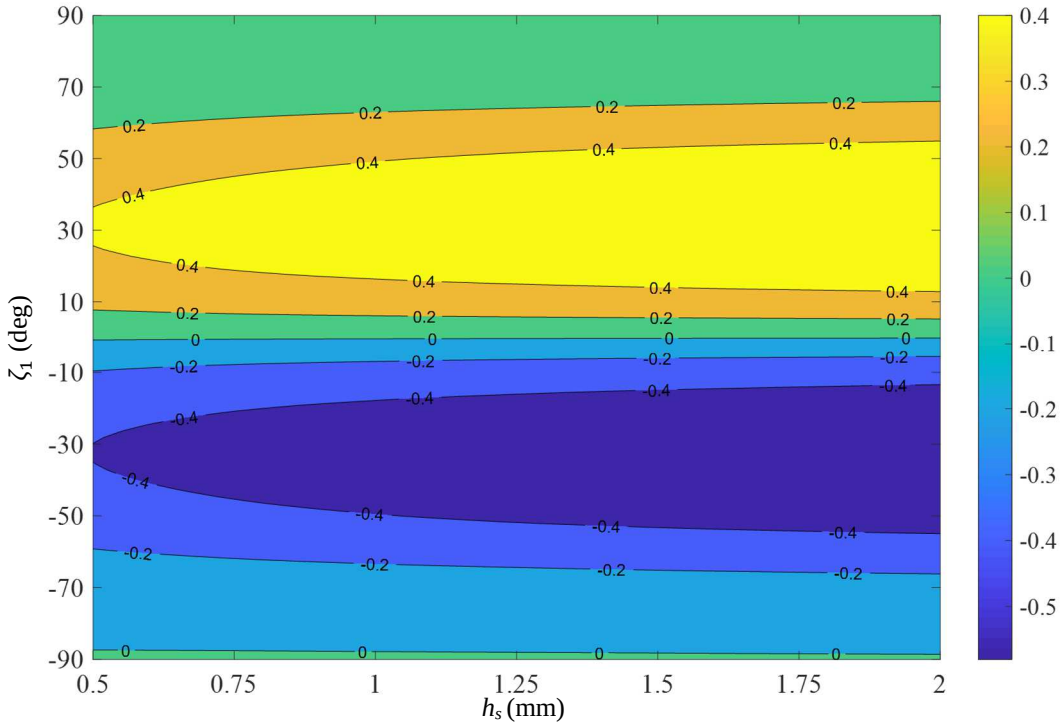

Figure 7: Contour plot of α showing effect of skin thickness and ζ_1 on the nondimensional bend-twist coupling

The simultaneous effects of spar location and skin ply angle on the bend-twist coupling is determined and shown in Figure 8. The ply angle range which results in the highest coupling is the same as Figure 7. In this range of skin ply angles, by moving the spar location to the leading edge of the blade, the nondimensional coupling value increases slightly.

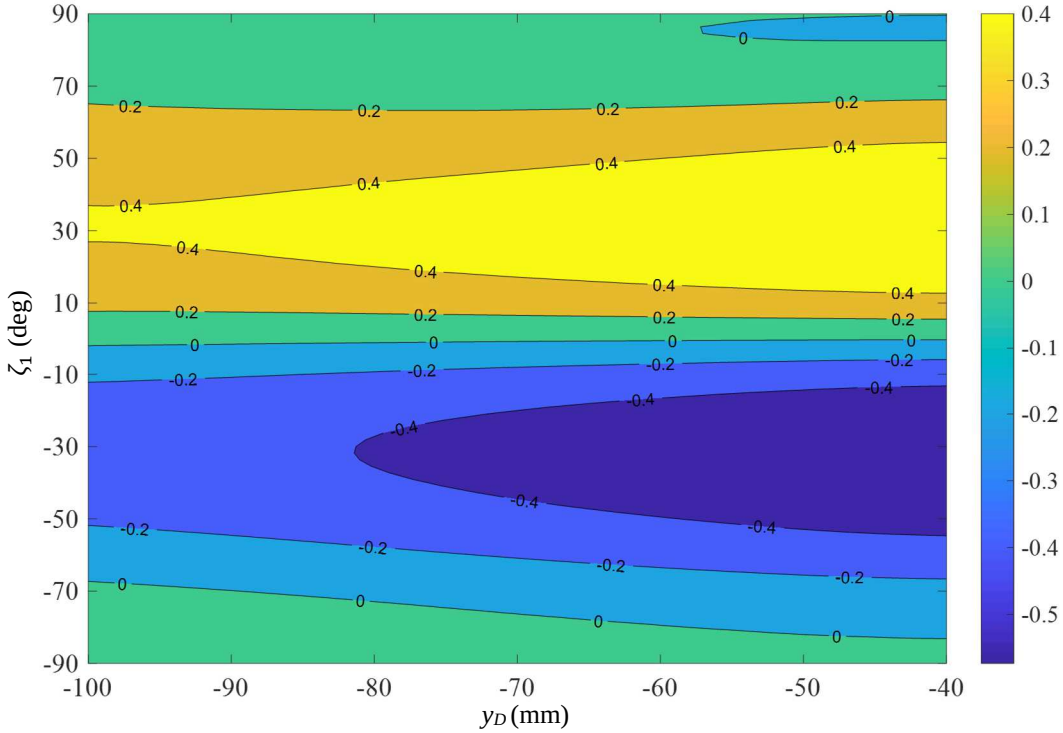

Figure 8: Contour plot of α showing effect of spar location and ζ_1 on the nondimensional bend-twist coupling

Finally, the mutual effect of the skin thickness and spar location on the nondimensional coupling is plotted in Figure 8. There are two domains where change occurs here. In the first region, where $-60<y_D<-40$, by increasing the skin thickness, the coupling value increases. In contrast, in the range of spar location where $-100<y_D<-60$, by increasing the skin thickness, the nondimensional coupling value decreases. This highlights that all the parameters are effective in optimizing the nondimensional bend-twist coupling.

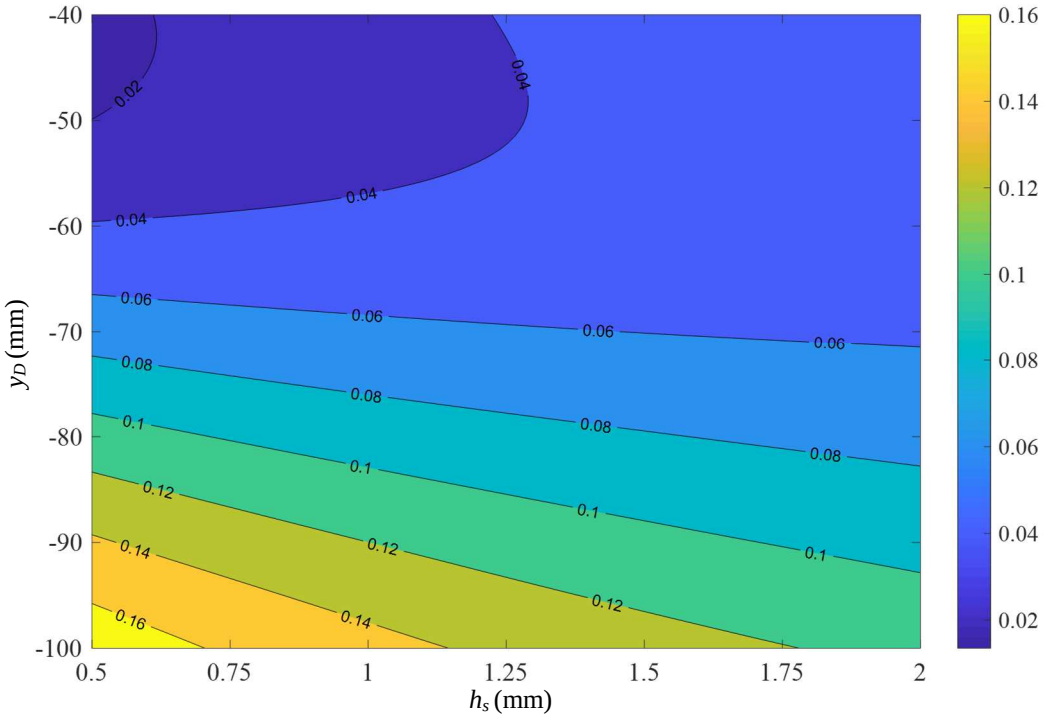

Figure 9: Contour plot of α showing effect of skin thickness and spar location on the nondimensional bend-twist coupling

Table 6: Baseline and optimized designs

Design variable	Baseline	Case 1	Case 2	Case 3
ζ_1(deg)	79	-75	-83	36
ζ_2 (deg)	63	34	34	-85
ζ_3 (deg)	22	-6	67	28
ζ_4 (deg)	39	42	63	89
ζ_5 (deg)	73	68	80	36
ζ_6 (deg)	-84	-76	43	39
ζ_7 (deg)	37	89	70	88
ζ_8 (deg)	-73	21	17	19
ζ_9 (deg)	85	-64	0	19
ζ_{10} (deg)	-28	12	31	18
ζ_{11} (deg)	-30	6	67	18
ζ_{12} (deg)	67	2	31	17
h_s(mm)	1.5	1.09	1.25	0.62
h_D(mm)	4.5	1.47	2.9	4.2
y_D (mm)	-49	-43	-40	-71
ω_{L1}(/rev)	0.64	0.70	0.71	0.65
ω_{F1}(/rev)	1.022	1.022	1.022	1.023
ω_{T1}(/rev)	3.69	3.77	3.72	3.61
$\lvert\alpha\rvert$	0.18	0.6	0.62	0.59

By considering the constraints on the blade fundamental natural frequencies, the optimization problem is solved to achieve the highest feasible bend-twist coupling value. The three best trade-off designs when constraining the

fundamental frequencies to be as close as possible to the baseline blade are given in Table 6. With these constraints, the maximum bend-twist coupling for the proposed configuration is approximately $\alpha = 0.6$.

The main cross-sectional properties of the optimal cases are presented in Table 7. It is noted here that in industry, it might not be possible to attain exactly these optimal values because of cost and manufacturability limitations. However, this study could give a deep insight on how the bend-twist coupling may change with respect to different cross-sectional parameters.

Table 7: Baseline and optimized designs cross-sectional properties

Design variable	Baseline	Case 1	Case 2	Case 3
D_{11} (N/m^2)	1.06×10^4	1.12×10^4	1.21×10^4	1.56×10^4
D_{22} (N/m^2)	2.94×10^3	4.44×10^3	4.7×10^3	4.88×10^3
D_{33} (N/m^2)	2.68×10^5	6.37×10^5	7.6×10^5	4.75×10^5
D_{13} (N/m^2)	9.89×10^3	5.12×10^4	5.9×10^4	5.07×10^4
μ (kg/m)	2.4	1.44	1.83	1.9
x_{ea} (%)	-22	-19	-20	-20

Conclusion

A composite blade cross-section was designed to have high value of bend-twist coupling. This coupling is introduced in the composite blade to change the twist of the blade. The blade twist can be changed by moving a mass in the chordwise direction of the blade. By moving the mass, a local centrifugal force is obtained which then turns into an equivalent torsional moment through the bend-twist coupling of the composite lay-up. The blade was modelled by using the geometrically exact fully intrinsic beam equations, and the cross-sectional properties of the blade was obtained by using a detailed cross-sectional analysis tool. A parametric cross-section was developed to capture the effective parameters of the section on the bend-twist coupling. Then a parametric sensitivity analysis carried out, and the most effective parameters were determined. It was found that the skin ply angle and thickness, and the spar location have the highest contribution on the bend-twist coupling of the composite lamination. Finally, three optimized cases subjected to the proposed constrains with highest possible bend-twist coupling were determined. It was highlighted that with the proposed configuration of the cross-section, the highest amount of the nondimensional bend-twist coupling is 0.6, which it can produce approximately 10^0 of maximum twist change when the point mass is equal to 5% mass of the blade.

Acknowledgements

The work presented in this paper was funded by the European Union Horizon 2020 Program through the project “Shape Adaptive Blades for Rotorcraft Efficiency (SABRE)”, Grant Agreement 723491.

References

1. Weisshaar TA. Morphing aircraft technology- New shapes for aircraft design. RTO-MP-AVT-141, Neuilly-sur-seine, France. 2006.
2. Barbarino S, Bilgen O, Ajaj RM, Friswell MI, Inman DJ. A Review of Morphing Aircraft. Journal of Intelligent Material Systems and Structures. 2011;22(9):823-77.
3. Reed JL, Hemmelgarn CD, Pelley BM, Havens E. Adaptive wing structures. Proceedings of SPIE Smart Structures and Materials 2005: Industrial and Commercial Applications of Smart Structures Technologies, 9 March, San Diego, CA, Vol 5762. 2005.
4. Markus K, Martin W, Peter MH, Olaf H, Timo K. Design of a smart leading edge device for low speed wind tunnel tests in the European project SADE. International Journal of Structural Integrity. 2011;2(4):383-405.
5. Woods BKS, Friswell MI. Preliminary Investigation of a Fishbone Active Camber Concept. 2012(45103):555-63.
6. Vale J, Leite A, Lau F, Suleman A. Aero-Structural Optimization and Performance Evaluation of a Morphing Wing with Variable Span and Camber. Journal of Intelligent Material Systems and Structures. 2011;22(10):1057-73.
7. Johnson W. Helicopter theory. Princton University Press, Princton, NJ1980.

8. Peter CC, Inderjit C. Induced strain actuation of composite beams and rotor blades with embedded piezoceramic elements. Smart Materials and Structures. 1996;5(1):35.
9. Chen PC, Chopra I. Hover Testing of Smart Rotor with Induced-Strain Actuation of Blade Twist. AIAA Journal. 1997;35(1):6-16.
10. Friedrich KS. A feasibility study of using smart materials for rotor control. Smart Materials and Structures. 1996;5(1):1.
11. Chopra I. Review of State of Art of Smart Structures and Integrated Systems. AIAA Journal. 2002;40(11):2145-87.
12. Chattopadhyay A, Liu Q, Gu H. Vibration Reduction in Rotor Blades Using Active Composite Box Beam. AIAA Journal. 2000;38(7):1125-31.
13. Carlos ESC, SangJoon S, Matthew LW. Dynamic response of active twist rotor blades. Smart Materials and Structures. 2001;10(1):62.
14. Shin S-J, Cesnik C. Forward flight response of the active twist rotor for helicopter vibration reduction. 19th AIAA Applied Aerodynamics Conference. Fluid Dynamics and Co-located Conferences: American Institute of Aeronautics and Astronautics; 2001.
15. Thakkar D, Ganguli R. Helicopter vibration reduction in forward flight with induced-shear based piezoceramic actuation. Smart Materials and Structures. 2004;13(3):599.
16. Schultz MR. A Concept for Airfoil-like Active Bistable Twisting Structures. Journal of Intelligent Material Systems and Structures. 2008;19(2):157-69.
17. Prahlad H, Chopra I. Design of a variable twist tilt-rotor blade using shape memory alloy (SMA) actuators. SPIE's 8th Annual International Symposium on Smart Structures and Materials. 2001.
18. Bushnell GS, Arbogast D, Ruggeri R. Shape control of a morphing structure (rotor blade) using a shape memory alloy actuator system. Proceedings of SPIE Smart Structures and Materials. 2008.
19. Pagano A, Ameduri S, Cokonaj V, Prachar A, Zachariadis Z, Drikakis D. Helicopter blade morphing strategies aimed at mitigating environmental impact. Jounral of Theoretical and Applied Mechanics. 2011;49(4):1233-59.
20. Mistry M, Gandhi F, Nagelsmit M, Gurdal Z. Actuation Requirements of a Warp-Induced Variable Twist Rotor Blade. Journal of Intelligent Material Systems and Structures. 2011;22(9):919-33.
21. Mistry M, Gandhi F. Design, fabrication, and benchtop testing of a helicopter rotor blade section with warp-induced spanwise camber variation. Journal of Intelligent Material Systems and Structures. 2015;26(10):1272-89.
22. Amoozgar MR, Shaw AD, Zhang J, Friswell MI. Twist morphing of a hingeless rotor blade using a moving mass. Proceedings of the 44th European Rotorcraft Forum, Delft. 2018.
23. Smith EC, Chopra I. Formulation and Evaluation of an Analytical Model for Composite Box-Beams. Journal of the American Helicopter Society. 1991;36(3):23-35.
24. Li L, Volovoi VV, Hodges DH. Cross-Sectional Design of Composite Rotor Blades. Journal of the American Helicopter Society. 2008;53(3):240-51.
25. Cesnik CES, Mok J, Morillo JA, Parikh AS. Design optimization of active twist rotor blades. Proceedings of the 30th European Rotorcraft Forum, Marseilles. 2004.
26. Glaz B, Friedmann P, Liu L, Kumar D, Cesnik C. The AVINOR Aeroelastic Simulation Code and Its Application to Reduced Vibration Composite Rotor Blade Design. 50th AIAA/ASME/ASCE/AHS/ASC Structures, Structural Dynamics, and Materials Conference. 2009.
27. Hodges DH. Geometrically Exact, Intrinsic Theory for Dynamics of Curved and Twisted Anisotropic Beams. AIAA Journal. 2003;41(6):1131-7.
28. Amoozgar M, Shahverdi H. Dynamic Instability of Beams Under Tip Follower Forces Using Geometrically Exact, Fully Intrinsic Equations. Latin American Journal of Solids and Structures. 2016;13:3022-38.
29. Amoozgar MR, Shahverdi H. Analysis of nonlinear fully intrinsic equations of geometrically exact beams using generalized differential quadrature method. Acta Mechanica. 2016;227(5):1265-77.
30. Amoozgar MR, Shahverdi H, Nobari AS. Aeroelastic Stability of Hingeless Rotor Blades in Hover Using Fully Intrinsic Equations. AIAA Journal. 2017;55(7):2450-60.
31. Mardanpour P, Hodges DH, Neuhart R, Graybeal N. Engine Placement Effect on Nonlinear Trim and Stability of Flying Wing Aircraft. Journal of Aircraft. 2013;50(6):1716-25.

32. Sotoudeh Z, Hodges DH. Structural Dynamics Analysis of Rotating Blades Using Fully Intrinsic Equations, Part I: Formulation and Verification of Single-Load-Path Configurations. Journal of the American Helicopter Society. 2013;58(3):1-9.
33. Yu W, Hodges DH, Volovoi V, Cesnik CES. On Timoshenko-like modeling of initially curved and twisted composite beams. International Journal of Solids and Structures. 2002;39(19):5101-21.